Arabian Journal of Chemistry (2016) 9, S678–S684

King Saud University

Arabian Journal of Chemistry

www.ksu.edu.sa
www.sciencedirect.com

ORIGINAL ARTICLE

Effect of Fe_2O_3 precursors on physicochemical and catalytic properties of CuO/Fe_2O_3 system

Nabil H. Amin *, Laila I. Ali, Sahar A. El-Molla, Anwer A. Ebrahim, Hala R. Mahmoud

Chemistry Department, Faculty of Education, Ain Shams University, Roxy, Heliopolis, Cairo 11757, Egypt

Received 13 May 2011; accepted 22 July 2011
Available online 31 July 2011

KEYWORDS

Amorphous materials;
H_2O_2 decomposition;
Catalysis;
FT-IR;
X-ray diffraction

Abstract CuO/Fe_2O_3 catalysts were prepared by impregnation method and calcined at 400 °C. The effect of changing the precursors of Fe_2O_3 and CuO loading on thermal, crystal, surface, spectral and catalytic properties of the catalysts were characterized by TG/DTG/DTA, XRD, N_2-adsorption at −196 °C, FT-IR and the catalytic decomposition of H_2O_2 at 30 °C. The results obtained revealed that the investigated catalysts consisted of nanosized Fe_2O_3 as a major phase besides $CuFe_2O_4$ phase. The precursor of Fe_2O_3 (nitrate or sulfate) affects the thermal properties of CuO/Fe_2O_3 system. The S_{BET} of CuO/Fe_2O_3 system calcined at 400 °C increases with using nitrate precursor of Fe_2O_3. The catalytic activity of H_2O_2 decomposition on all $CuFeO_n$ catalysts (nitrate precursor) is higher than that of $CuFeO_s$ catalysts (sulfate precursor).

1. Introduction

Metal oxides are interesting solids due to their surface acid–base properties (Khaleel et al., 2010) and oxidation–reduction potentials (Cao et al., 2008). Therefore, they constitute the largest family of heterogeneous catalysts. The oxidation–reduction behavior of several transition metal oxides is due to the ease with which they are alternately reduced and oxidized which means that they can be used as oxidizing agents and then readily be regenerated (Khaleel and Al-Nayli, 2008). Iron (III) oxide, α-Fe_2O_3, and several iron oxide-based catalysts are of significant importance in catalysis, especially in oxidation processes (Al-Sayari et al., 2007; Wang et al., 2008). Besides its catalytic potential, α-Fe_2O_3 is used for many applications because of its non-toxicity, low processing cost, availability, and high resistance to oxidative change (Cao et al., 2008; Liu et al., 2008; Mishra and Parida, 2006). Their disadvantages are low thermal stability against sintering and crystal growth which are typically accompanied by considerable surface area reduction and, hence, rapid deactivation in catalytic investigations (Liu et al., 2008). Therefore, modification of iron oxide by mixing it with other oxides attracted the attention of many researchers (Cao et al., 2008; Liu et al., 2008; Mishra and Parida, 2006). Mixed oxide catalysts usually

* Corresponding author. Tel.: +20 19 2609104; fax: +20 02 22581243.
E-mail address: nabil_egypt92@yahoo.com (N.H. Amin).
Peer review under responsibility of King Saud University.

Production and hosting by Elsevier

http://dx.doi.org/10.1016/j.arabjc.2011.07.026
1878-5352

exhibit modified textural, structural, and catalytic properties as compared with their corresponding metal oxide (Wachs, 2005). A mixed metal oxide catalyst, copper oxide/iron oxide (CuO/Fe_2O_3) was selected as potential volatile organic compounds' (VOCs) oxidation catalyst (Minico et al., 2000), carbon monoxide (CO) oxidation (Cao et al., 2008), hydrogen production reactions (Chang et al., 2009), organic oxidation reactions (Litt and Almquist, 2009), and peroxide decomposition reactions (Shaheen, 2001).

Catalytic decomposition of H_2O_2 is an oxidation–reduction reaction, one of its applications as a green fuel/propellant instead of carcinogenic hydrazine in spaceflight at certain conditions (Teshimal et al., 2004). Hydrogen peroxide (H_2O_2) can be used as an oxidizer in the fuel cells (Sanli and Aytac, 2011). The oxidative removal of natural organic matter (NOM) from water takes place by using hydrogen peroxide (Kitis and Kaplan, 2007). Furthermore, hydrogen peroxide has none of the environmental problems associated with most other chemical oxidizers (Selvarani et al., 2008). After learning that hydrogen peroxide could be made from water and solar energy, it was decided that H_2O_2 would be a suitable alternative fuel (Wee, 2006).

The catalyst preparation conditions, such as precursor, calcination temperature and doping can affect the catalyst properties, including surface area, morphology, crystallinity, and dispersion (Litt and Almquist, 2009; El-Molla et al., 2009; Amin, 2000).

In this paper, we aimed to investigate the effect of iron oxide precursors at different CuO loading to CuO/Fe_2O_3 system on the catalytic activity of H_2O_2 decomposition.

2. Experimental

2.1. Material and methods

Iron hydroxides were precipitated from both of iron nitrate $Fe(NO_3)_3{\cdot}9H_2O$ (1 M) solution and iron sulfate $Fe_2(SO_4)_3$ (1 M) solution using ammonia solution (0.2 M) at 70 °C and pH = 8. The precipitates were carefully washed with bi-distilled water till free from ammonium and nitrate or sulfate ions, then filtered and dried at 110 °C till constant weight. The formula of the prepared hydroxide precipitated from iron nitrate can be expressed as $Fe_2O_3{\cdot}1.5H_2O$ while that from iron sulfate can be expressed as $Fe_2O_3{\cdot}3H_2O$ (Pailhé et al., 2008). The catalysts were calcined in air at 400 °C for 4 h.

Nine specimens of CuO/Fe_2O_3 catalysts were prepared by wet impregnation method. A known mass of iron hydroxide was impregnated with solutions containing different amounts of copper nitrate dissolved in the least amount of bi-distilled water sufficient to make pastes which were dried at 110 °C followed by calcination at 400 °C for 4 h. The nominal compositions of the impregnated catalysts from nitrate precursor were 0.05, 0.10, 0.15, $0.20CuO/Fe_2O_3$, which correspond to 2.42, 4.73, 6.94, and 9.04 wt% CuO, respectively. The nominal compositions of the impregnated catalysts from sulfate precursor were 0.025, 0.035, 0.050, 0.075, $0.100CuO/Fe_2O_3$, which correspond to 1.23, 1.71, 2.42, 3.59, and 4.73 wt% CuO, respectively.

The all catalysts prepared from nitrate and sulfate precursors were nominated as XCuFeO$_n$ and XCuFeO$_s$ (X is the CuO concentration), respectively. All chemicals used in the experiment were of analytical grade.

2.2. Characterization techniques

Thermogravimetric (TG), differential thermogravimetric (DTG), and differential thermal analysis (DTA) curves of the catalysts were obtained using Shimadzu TGA/DTA-50H thermogravimetric analyzer, the rate of heating was kept at 10 °C/min, and the flow rate of nitrogen was 30 ml/min.

X-ray diffractograms of various prepared solids were determined a Brucker diffractometer (Brucker Axs D8 Advance Germany). The patterns were run with CuKα_1 with secondly monochromator (λ = 0.15404 Å) at 40 kV and 40 m A at a scanning rate of 2° in 2θ/min.

The infrared transmission spectra of various solids were determined by FT-IR spectroscopy (Jasco FT-IR 4100 spectrometer (Japan)) employing samples prepared as KBr disks. The IR spectra were measured from 400 to 4000 cm^{-1}. The most important and characteristic absorption bands thus determined were compared with those reported in the literature.

The specific surface area (S_{BET}) of the prepared catalysts were determined from nitrogen adsorption isotherms measured at −196 °C using a Quantachrome NOVA 2000 automated gas-sorption apparatus model 7.11. All catalysts were degassed at 200 °C for 2 h under a reduced pressure of 10^{-5} Torr before undertaking such measurements.

The catalytic activities of the various catalysts were measured by studying the decomposition of H_2O_2 in their presence at 30 °C using 100 mg of a given catalyst sample with 0.5 ml of H_2O_2 of known concentration diluted to 20 ml with distilled water. The reaction kinetics was monitored by measuring the volume of O_2 liberated at different time intervals until no further oxygen was liberated.

3. Results and discussion

3.1. Thermal properties

TG/DTG and DTA-curves of uncalcined 0.05CuFeO$_n$ and 0.05CuFeO$_s$ catalysts are shown in Figs. 1(A, B) and 2(A, B), respectively, and the data are listed in Table 1. It is shown that (i) the TG-curves of 0.05CuFeO$_n$ and 0.05CuFeO$_s$ catalysts were the same and consist of three stages. The first and second steps characterized the departure of physisorbed water and some water of crystallization of iron hydroxide with a complete thermal decomposition of copper nitrate into copper oxide CuO (Deraz, 2008). The last step indicated the complete decomposition of iron hydroxide into iron oxide Fe_2O_3. (ii) Three endothermic peaks were obtained from the DTA-curves of the 0.05CuFeO$_n$ and 0.05CuFeO$_s$ catalysts which correspond to the removal of water of crystallization, decomposition of copper nitrate and iron hydroxide, respectively. Two exothermic peaks were also obtained from DTA-curves, due to the formation of copper ferrite. (iii) It was clear that the thermal evolution of the sulfate precursor toward the formation of different oxides (copper, iron) and spinel phase ($CuFe_2O_4$) was slower than the nitrate precursor (Martín de Vidalesa et al., 1999).

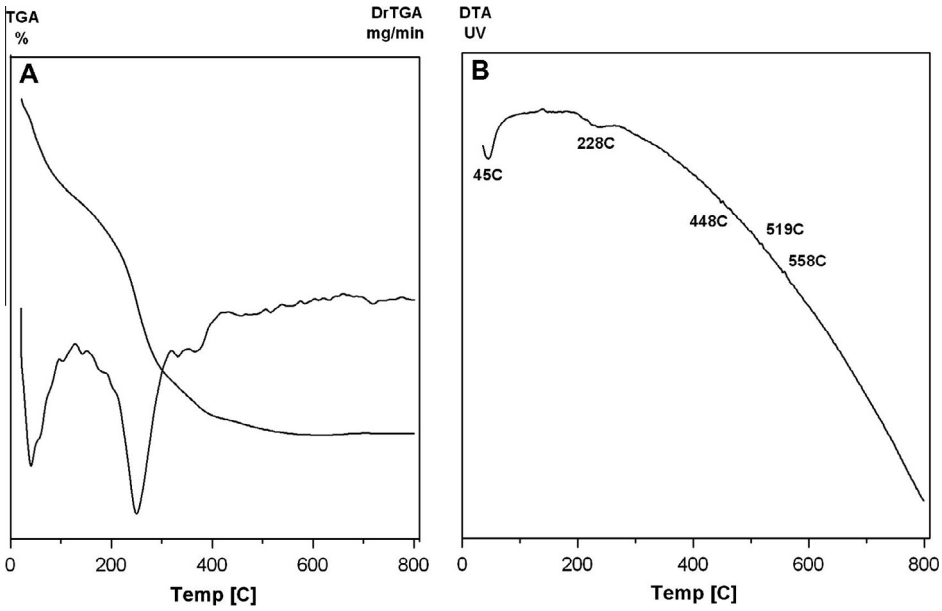

Figure 1 Thermograms of uncalcined $0.05CuFeO_n$ catalysts: (A) TG/DTG and (B) DTA.

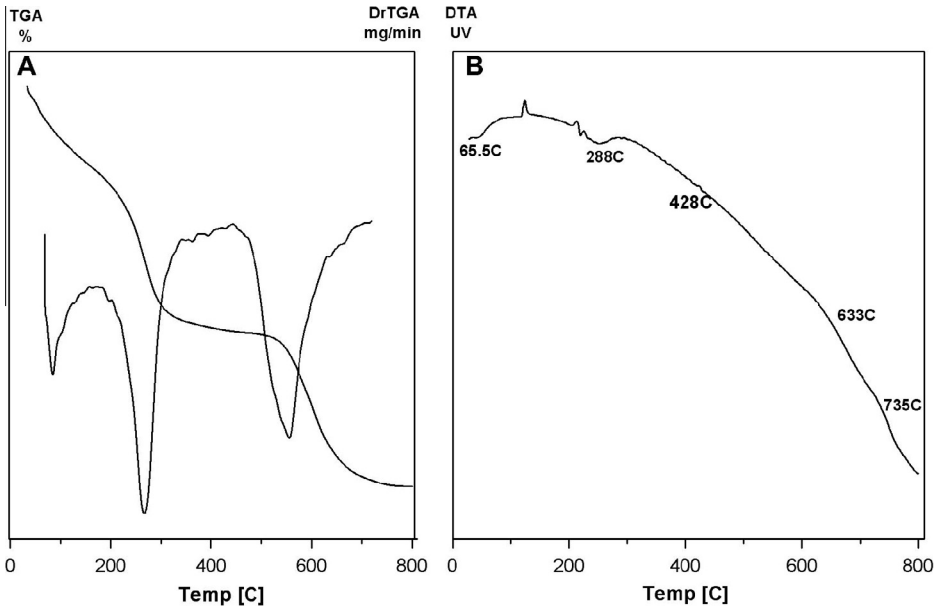

Figure 2 Thermograms of uncalcined $0.05CuFeO_s$ catalysts: (A) TG/DTG and (B) DTA.

Table 1 Effect of changing precursor of Fe_2O_3 on the thermal behavior of uncalcined $0.05CuO/Fe_2O_3$ catalysts.

Catalyst	$0.05CuFeO_n$	$0.05CuFeO_s$
T_1 (°C) (weight loss %)	Rt → 86 (3.5)	Rt → 87 (3.2)
T_2 (°C) (weight loss %)	87 → 305 (9)	88 → 303 (12.6)
T_3 (°C) (weight loss %)	306 →782 (2.8)	304 →799 (12.9)
Calculated total weight loss %	18.3	29.6
Found total weight loss %	15.3	28.7
T (°C) of endothermic peaks	45, 228, 448	65.5, 288, 428
T (°C) of exothermic peaks	519, 558	633, 735

Rt: room temperature.

(iv) The difference between the total practical weight loss and theoretical value is attributed to the removal of surface hydroxyl groups which need thermal treatment ⩾ 800 °C (Cao et al., 2008).

3.2. Crystal structure and surface properties

3.2.1. XRD analysis

The XRD patterns of $0.05CuFeO_n$, $0.20CuFeO_n$, $0.05CuFeO_s$, and $0.10CuFeO_s$ catalysts being calcined at 400 °C were determined and illustrated in Fig. 3. It is seen that all of the detectable peaks at 2θ = 33.1, 41.1, 49.5, 54.1, and 64° can be

indexed to the Fe_2O_3 hematite phase (JCPDS 33-0664). Also, another peaks at $2\theta = 35.6$ and 62.6° can be indexed to the $CuFe_2O_4$ phase (JCPDS 34-0425). No CuO phase was observed in the XRD patterns of the investigated catalysts due to diffusion of CuO into the matrix of α-Fe_2O_3 forming copper ferrite $CuFe_2O_4$ phase, monolayer dispersion of CuO on the surface of α-Fe_2O_3 and/or complete amorphization of CuO (Jiang et al., 2005).

The effects of changing the Fe_2O_3 precursors on the degree of ordering and the crystallite sizes of different phases in the investigated catalysts were emerged from the data listed in Table 2. Inspection of Table 2 shows the following: (i) the diffractograms of $CuFeO_n$ and $CuFeO_s$ consist of Fe_2O_3 and $CuFe_2O_4$ with a moderate degree of ordering. (ii) Increasing of CuO loading on Fe_2O_{3n} was accompanied by decreasing the degree of ordering and the crystallite sizes of hematite phase while increasing in the case of copper ferrite phase. (iii) Increasing of CuO loading on Fe_2O_{3s} was accompanied by increasing the degree of ordering and the crystallite sizes of hematite and copper ferrite phases. The smallest degree of ordering was found in $CuFeO_s$ (sulfate precursor). All phases present in the investigated catalysts have nano-crystallite sizes $\leqslant 24$ nm. (iv) The degree of ordering and the crystallite sizes of Fe_2O_3 phase in $0.05CuFeO_n$ were higher than those of $0.05CuFeO_s$ catalysts.

The explanation of different behavior of $0.05CuFeO_s$ with comparison to $0.05CuFeO_n$ catalysts may be due to the difference in the thermal properties as shown in (TG-DTG-DTA) analysis section. This could be attributed to the lower thermal stability of the uncalcined $0.05CuFeO_n$ catalyst relative to $0.05CuFeO_s$ catalyst.

3.2.2. Surface properties

The specific surface areas of the investigated catalysts calcined in air at 400 °C were determined from nitrogen adsorption isotherms conducted at −196 °C. Specific surface areas (S_{BET}) calculated for various adsorbents are listed in Table 2. Inspection of the results in Table 2 shows that (i) the S_{BET} of Fe_2O_{3n} was significantly enhanced by loading 2.42 wt% CuO. This behavior can be explained by creation of new pores during the liberation of nitrogen oxide gases during the thermal decomposition of copper nitrate (Radwan et al., 2004;

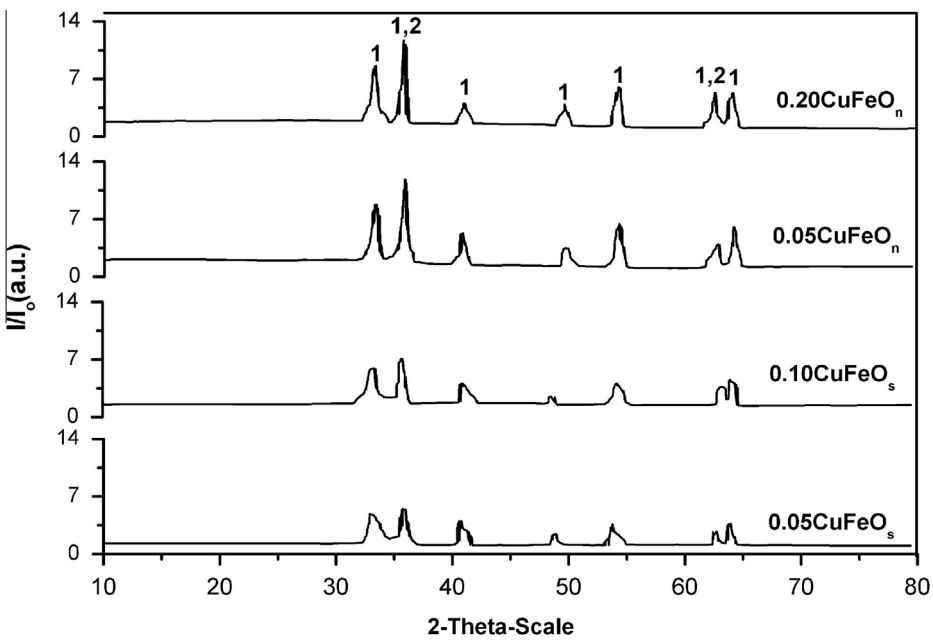

Figure 3 XRD patterns of CuFeO catalysts prepared from different Fe_2O_3 precursors calcined at 400 °C. Lines (1) refer to α-Fe_2O_3 and lines (2) refer to $CuFe_2O_4$ phases.

Table 2 Intensity counts of the main diffraction lines, crystallite size of various phases and S_{BET} for the investigated catalysts calcined at 400 °C.

Catalyst	Intensity count (a.u.)		Crystallite size (nm)		S_{BET} (m^2/g)
	Fe_2O_3	$CuFe_2O_4$	Fe_2O_3	$CuFe_2O_4$	
Fe_2O_{3n}	–	–	–	–	27.5
$0.05CuFeO_n$	8.7	7.9	12.4	16.3	84.6
$0.20CuFeO_n$	8.5	8.5	10.6	23.7	71.2
$0.05CuFeO_s$	4.6	4	6.9	24.3	52.3
$0.10CuFeO_s$	5.6	5.5	7.1	18.3	–

–: not measured.

Avgouropoulos and Ioannides, 2003) and fine dispersion of CuO particles on the surface of hematite. Further loading of 9.04 wt% CuO on Fe_2O_{3n} leads to dissipation in the S_{BET} value with about 15.8% due to the aggregation of small copper species during preparation process (Wang et al., 2002). (ii) $0.05CuFeO_s$ prepared from sulfate precursor had the smallest S_{BET} value. (iii) The S_{BET} of $0.05CuFeO_n$ catalyst prepared from the nitrate precursor was the biggest one. This event can be related to the crystallite sizes of $CuFe_2O_4$ phase in $0.05CuFeO_s$ (24.3 nm) which were bigger than those in $0.05CuFeO_n$ (16.3 nm).

3.3. Spectral properties

Fig. 4(A and B) shows the FT-IR spectra of pure α-Fe_2O_3 obtained from thermal decomposition of iron hydroxides precipitated from iron nitrate and iron sulfate (α-Fe_2O_{3n}, α-Fe_2O_{3s}) in air at 400 °C, respectively. Sample (A) showed absorption in the regions 3417, 1619, 540, and 455 cm^{-1}. Sample (B) showed absorption in the regions 3414, 1626, 1121, 537, and 450 cm^{-1}. The general range of 3600–3100 cm^{-1} may be assigned to antisymmetrical and symmetrical O–H bonding stretching vibrational modes for water of hydration (Apte et al., 2007). The bonding in the region of 1670–1600 cm^{-1} also relates to O–H bonding bending vibrational modes (Apte et al., 2007). The bands at 455 and 540 cm^{-1} observed in two samples can be attributed to metal oxygen stretching vibrational modes (Apte et al., 2007). In addition, the spectrum of α-Fe_2O_{3s} showed a band at 1121 cm^{-1} arising from the symmetric stretching mode of SO_4 anion (Zhang et al., 2006). No NO_3 anion band is observed in FT-IR spectrum of α-Fe_2O_{3n}.

3.4. Catalytic activity

Catalytic decomposition of H_2O_2 is a model reaction chosen to study the redox properties of the prepared catalysts. Fig. 5(A and B) shows the first-order plots of catalytic decomposition of H_2O_2 conducted at 30 °C over $CuFeO_n$ and $CuFeO_s$ catalysts at different CuO loading calcined at 400 °C, respectively. The variation of reaction rate constant (k) as a function of wt% of CuO for the $CuFeO_n$ and $CuFeO_s$ catalysts precalcined at 400 °C is graphically represented in Fig. 6(A and B), respectively. It is shown from Fig. 5(A and B) that (i) the catalytic activity of all $CuFeO_n$ and $CuFeO_s$ catalysts is higher than the pure Fe_2O_3 catalyst. (ii) The catalytic activity of $CuFeO_n$ catalysts is higher than $CuFeO_s$ catalysts at all CuO loadings. Inspection of Fig. 6(A and B) revealed that (i) the increase in amount of CuO content from 2.42 to 9.04 wt% is accompanied with a progressive increasing of the catalytic activity of $CuFeO_n$ catalysts calcined at 400 °C. (ii) The catalytic activity of $CuFeO_s$ catalysts increases progressively by increasing the amounts of CuO up to a certain extent reaching to a maximum at 2.42 wt% of CuO. Further increase in the amount of CuO 2.42 wt% was followed by a decrease in the catalytic activity.

The observed increase in the catalytic activity of all CuFeO catalysts calcined at 400 °C in comparison to pure Fe_2O_3 can be interpreted in terms of the concept of bivalent catalytic centers (Shaheen, 2007) such as Cu^{2+}–Fe^{3+} and/or Cu^{1+}–Fe^{2+} ion pairs beside the one component sites Cu^{2+}–Cu^{+1}, Fe^{3+}–Fe^{2+}. The presence of Cu^{2+}–Fe^{3+} and/or Cu^{1+}–Fe^{2+} ion pairs is a result of mutual charge interaction that is involved in H_2O_2-decomposition reaction (Shaheen, 2008). From the electronic theory of catalysis and the principle of bivalent catalytic sites there are two kinds of catalytic sites in equilibrium on the catalyst surface, i.e. donor and acceptor sites, which may be formed by metal catalyst ions in various valence states (depending on oxidation or reduction potential of each cation relative to that of H_2O_2) or by charge defects stabilized on the catalyst surface. Therefore, the catalytic reactions proceed on the catalytic sites constituted from the ion pairs (Fe^{3+}–Fe^{2+}) and/or (Cu^{2+}–Cu^{+1}) where one of the ions occurs in a lower and the second ion in a higher oxidation state (Radwan, 2004; Hasan et al., 1999; Radwan, 2006).

Alternatively, the modification of the surface area of the catalysts might be another critical reason for promoting the catalytic activity (see Table 2). Also, this behavior was due to greater lattice oxygen mobility in the mixed oxide catalysts than single one. The presence of Cu decreases the strength of

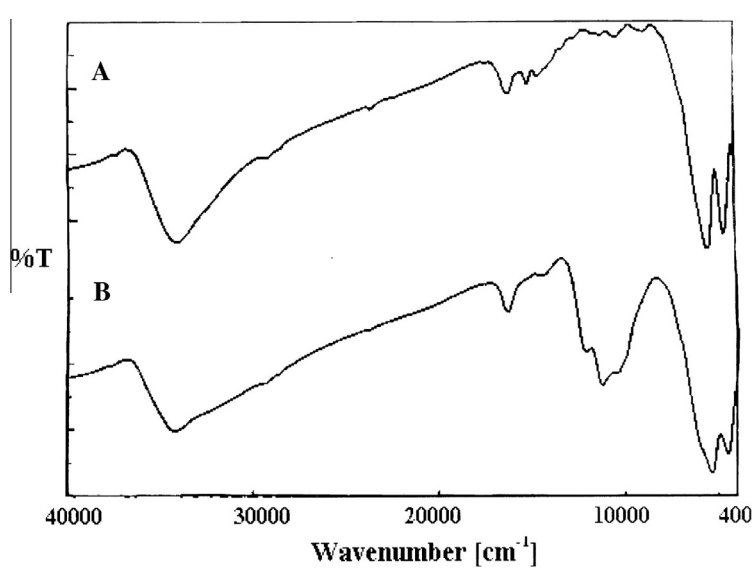

Figure 4 IR spectra of (A) α-Fe_2O_{3n} and (B) α-Fe_2O_{3s} catalysts calcined at 400 °C.

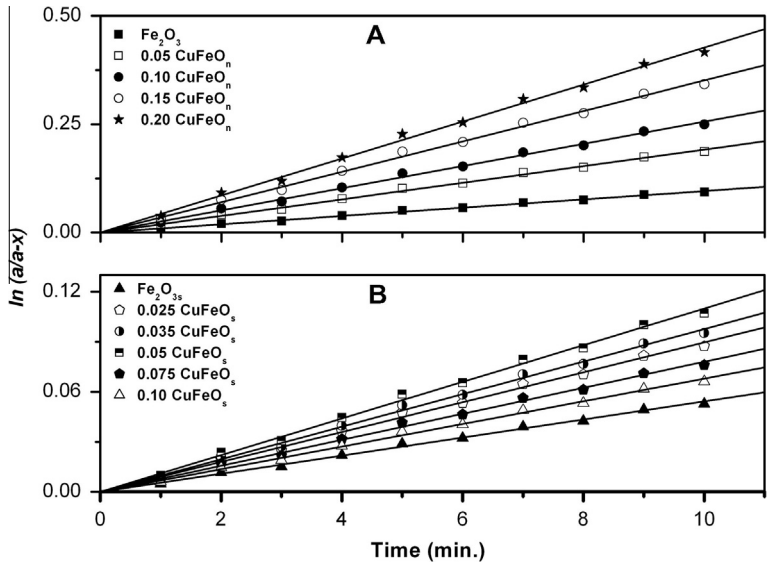

Figure 5 First-order plots of H_2O_2 decomposition conducted at 30 °C over (A) $CuFeO_n$ and (B) $CuFeO_s$ catalysts at different CuO loading calcined at 400 °C.

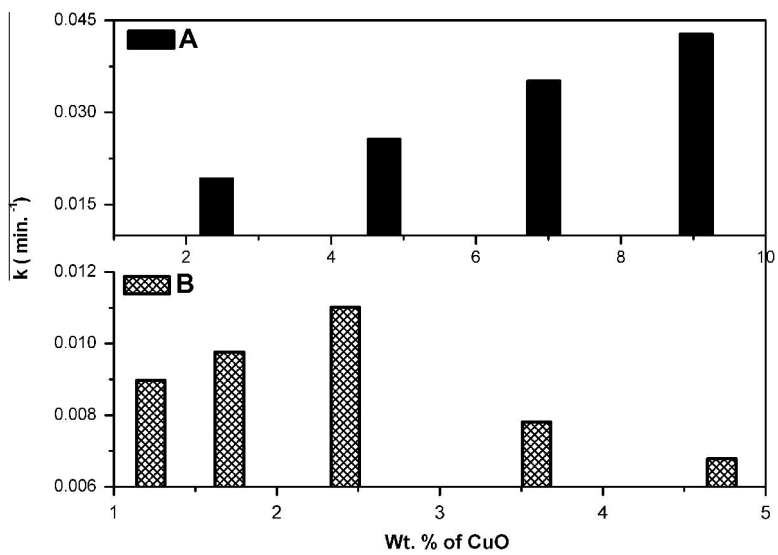

Figure 6 Variation of reaction rate constant (k) as a function of the wt% of CuO for the catalytic decomposition of H_2O_2 conducted at 30 °C over (A) $CuFeO_n$ and (B) $CuFeO_s$ catalysts calcined at 400 °C.

nearly Fe–O bonds, thus increasing the mobility of lattice oxygen and facilitating redox reactions on the catalyst surface (Litt and Almquist, 2009).

Changing the precursor of Fe_2O_3 as shown in $CuFeO_n$ increased the catalytic activity. The catalytic activity of $CuFeO_n$ is higher than $CuFeO_s$ catalysts at all CuO loadings. This could be attributed to the presence of traces of sulfate anions in $CuFeO_s$ catalysts as shown from FT-IR section. The presence of SO_4^{-2} ions leads to increase of the reaction solution acidity and then decrease of the H_2O_2-decomposition rate (Zhang et al., 2006). These results agree with the results of Schumb et al., (1955) which reported that the hydrogen peroxide is more stable at low pH. In addition, the SO_4^{-2} ions can adsorb strongly on the iron oxide surface instead of surface hydroxyl groups, especially at low SO_4^{-2} concentrations (Martin and Smart, 1987). This leads to the formation of a surface complex between SO_4^{-2} and α-FeOOH. This surface complex inhibits the catalytic decomposition of H_2O_2, possibly by affecting the surface charge or redox potential at the catalyst surface by decreasing H_2O_2 adsorption on decomposition sites (Watts et al., 1999; Sigg and Stumm, 1981; Choudhary et al., 2006; El-Shobaky et al., 2001).

4. Conclusions

The precursor of iron (nitrate or sulfate) affects the thermal, structural, and spectral properties of CuO/Fe_2O_3 system. The S_{BET} of CuO/Fe_2O_3 system calcined at 400 °C is significantly enhanced in the case of nitrate precursor of Fe_2O_3 in

comparison to sulfate precursor. Catalysts based on nitrate precursor exhibit high catalytic decomposition of H_2O_2 relative to catalysts based on sulfate precursor.

References

Al-Sayari, S., Carley, A.F., Taylor, S.H., Hutchings, G.J., 2007. Au/ZnO and Au/Fe_2O_3 catalysts for CO oxidation at ambient temperature: comments on the effect of synthesis conditions on the preparation of high activity catalyst prepared by coprecipitation. Top. Catal. 44, 123–127.

Amin, N.H., 2000. Some physicochemical, surface and catalytic properties of the MoO_3/Al_2O_3 system. Adsorp. Sci. Technol. 18, 409–419.

Apte, S.K., Naik, S.D., Sonawane, R.S., Kalew, B.B., 2007. Synthesis of nanosize-necked structure α- and γ-Fe_2O_3 and its photocatalytic activity. J. Am. Ceram. Soc. 90, 412–414.

Avgouropoulos, G., Ioannides, T., 2003. Selective CO oxidation over CuO–CeO_2 catalysts prepared via the urea–nitrate combustion method. Appl. Catal. A 244, 155–167.

Cao, J.-L., Wang, Y., Yu, X.-L., Wang, S.-R., Wu, S.-H., Yuan, Z.-Y., 2008. Mesoporous CuO–Fe_2O_3 composite catalysts for low-temperature carbon monoxide oxidation. Appl. Catal. B 79, 26–34.

Chang, F.-W., Ou, T.-C., Roselin, L.S., Chen, W.-S., Lai, S.-C., Wu, H.-M., 2009. Production of hydrogen by partial oxidation of methanol over bimetallic Au–Cu/TiO_2–Fe_2O_3 catalysts. J. Mol. Catal. A 313, 55–64.

Choudhary, V.R., Samanta, C., Choudhary, T.V., 2006. Factors influencing decomposition of H_2O_2 over supported Pd catalyst in aqueous medium. J. Mol. Catal. A 260, 115–120.

Deraz, N.M., 2008. Production and characterization of pure and doped copper ferrite nanoparticles. J. Anal. Appl. Pyrolysis 82, 212–222.

El-Molla, S.A., Abdel-all, S.M., Ibrahim, M.M., 2009. Influence of precursor of MgO and preparation conditions on the catalytic dehydrogenation of *iso*-propanol over CuO/MgO catalysts. J. Alloys Compd. 484, 280–285.

El-Shobaky, G.A., Amin, N.H., Deraz, N.M., El-Molla, S.A., 2001. Decomposition of H_2O_2 on pure and ZnO-treated Co_3O_4/Al_2O_3 solids. Adsorp. Sci. Technol. 19 (1), 45–58.

Hasan, M.A., Zaki, M.I., Pasupulety, L., Kumarik, K., 1999. Promotion of the hydrogen peroxide decomposition activity of manganese oxide catalysts. Appl. Catal. A 181, 171–179.

Jiang, J.S., Yang, X.L., Gao, L., Guo, J.K., 2005. Nanostructured CuO–α-Fe_2O_3 solid solution obtained by high-energy ball-milling. Mater. Sci. Eng. A 392, 179–183.

Khaleel, A., Al-Nayli, A., 2008. Supported and mixed oxide catalysts based on iron and titanium for the oxidative decomposition of chlorobenzene. Appl. Catal. B 80, 176–184.

Khaleel, A., Shehadil, I., Al-Shamisi, M., 2010. Nanostructured chromium–iron mixed oxides: physicochemical properties and catalytic activity. Colloids Surf. A 355, 75–82.

Kitis, M., Kaplan, S.S., 2007. Advanced oxidation of natural organic matter using hydrogen peroxide and iron-coated pumice particles. Chemosphere 68, 1846–1853.

Litt, G., Almquist, C., 2009. An investigation of CuO/Fe_2O_3 catalysts for the gas-phase oxidation of ethanol. Appl. Catal. B 90, 10–17.

Liu, X.H., Shen, K., Wang, Y.G., Wang, Y.Q., Guo, Y.L., Guo, Z.L., Yong, Z., Lu, G.Z., 2008. Preparation and catalytic properties of Pt supported Fe–Cr mixed oxide catalysts in the aqueous-phase reforming of ethylene glycol. Catal. Commun. 9, 2316–2318.

Martin, R., Smart, R.T., 1987. X-ray photoelectron studies of anion adsorption on goethite. Soil Sci. Soc. Am. J. 51, 54–56.

Martín de Vidalesa, J.L., López-Delgado, A., Vilac, E., López, F.A., 1999. The effect of the starting solution on the physico-chemical properties of zinc ferrite synthesized at low temperature. J. Alloys Compd. 287, 276–283.

Minico, S., Scire, S., Crisafulli, C., Maggiore, R., Galvagno, S., 2000. Catalytic combustion of volatile organic compounds on gold/iron oxide catalysts. Appl. Catal. B 28, 245–251.

Mishra, T., Parida, K.M., 2006. Effect of sulfate on the surface and catalytic properties of iron–chromium mixed oxide pillared clay. J. Colloid Interface Sci. 301, 554–559.

Pailhé, N., Wattiaux, A., Gaudon, M., Demourgues, A., 2008. Correlation between structural features and vis–NIR spectra of α-Fe_2O_3 hematite and AFe_2O_4 spinel oxides (A = Mg, Zn). J. Solid State Chem. 181, 1040–1047.

Radwan, N.R.E., 2004. Modification of surface and catalytic properties of Fe_2O_3 due to doping with rare-earth oxides Sm_2O_3 and Y_2O_3. Appl. Catal. A 273, 21–33.

Radwan, N.R.E., 2006. Influence of La_2O_3 and ZrO_2 as promoters on surface and catalytic properties of CuO/MgO system prepared by sol–gel method. Appl. Catal. A 299, 103–121.

Radwan, N.R.E., El-Shobaky, G.A., Fahmy, Y.M., 2004. Cordierite as catalyst support for cobalt and manganese oxides in oxidation–reduction reactions. Appl. Catal. A 274, 87–99.

Sanli, A.E., Aytac, A., 2011. Response to Disselkamp: direct peroxide/peroxide fuel cell as a novel type fuel cell. Int. J. Hydrogen Energy 36, 869–875.

Schumb, W.C., Stratterfield, C.N., Wentworth, R.L., 1955. Hydrogen Peroxide. American Chemical Society, Rienholt Publishing, New York.

Selvarani, G., Prashant, S.K., Sahu, A.K., Sridhar, P., Pitchumani, S., Shukla, A.K., 2008. A direct borohydride fuel cell employing Prussian blue as mediated electron-transfer hydrogen peroxide reduction catalyst. J. Power Sources 178, 86–91.

Shaheen, W.M., 2001. Thermal solid–solid interaction and physicochemical properties of CuO–Fe_2O_3 system. Int. J. Inorg. Mater. 3, 1073–1081.

Shaheen, W.M., 2007. Thermal behaviour of pure and binary $Fe(NO_3)_3{\cdot}9H_2O$ and $(NH_4)_6Mo_7O_{24}{\cdot}4H_2O$ systems. Mater. Sci. Eng. A, 113–121.

Shaheen, W.M., 2008. Thermal solid–solid interactions and physicochemical properties of NiO/Fe_2O_3 system doped with K_2O. Thermochim. Acta 470, 18–26.

Sigg, L., Stumm, W., 1981. The interaction of anions and weak acid with the hydrous goethite (α-FeOOH) surface. Colloids Surf. 2, 101–117.

Teshimal, N., Genfa, Z., Dasgupta, P.K., 2004. Catalytic decomposition of hydrogen peroxide by a flow-through self-regulating platinum black heater. Anal. Chim. Acta 510, 9–13.

Wachs, I.E., 2005. Recent conceptual advances in the catalysis science of mixed metal oxide catalytic materials. Catal. Today 100, 79–94.

Wang, J.B., Lin, S.-C., Huang, T.-J., 2002. Selective CO oxidation in rich hydrogen over CuO/samaria-doped ceria. Appl. Catal. A 232, 107–120.

Wang, H.C., Chang, S.H., Hung, P.C., Hwang, J.F., Chang, M.B., 2008. Catalytic oxidation of gaseous PCDD/Fs with ozone over iron oxide catalysts. Chemosphere 71, 388–397.

Watts, R.J., Foget, M.K., Kong, S.-H., Teel, A.L., 1999. Hydrogen peroxide decomposition in model subsurface systems. J. Hazard. Mater. B 69, 229–243.

Wee, J.-H., 2006. Which type of fuel cell is more competitive for portable application: direct methanol fuel cells or direct borohydride fuel cells? J. Power Sources 161, 1–10.

Zhang, L., Zhu, J., Jiang, X., Evans, D.G., Li, F., 2006. Influence of nature of precursors on the formation and structure of Cu–Ni–Cr mixed oxides from layered double hydroxides. J. Phys. Chem. Solids 67, 1678–1686.